ISSN (Print) 1226-1750
ISSN (Online) 2233-6656
Journal of Magnetics 31(3), 323-332 (2026) https://doi.org/10.4283/JMAG.2026.31.3.323

Spike Formation in Ferrofluidic Interfacial Instability Under Various Magnetic Fields

Liu Li[1,2] and Decai Li[2]*

[1]*Guangzhou Mechanical Engineering Research Institute Co., Ltd, Guangzhou 510000, China*
[2]*Department of Mechanical Engineering, Tsinghua University, Beijing 100084, China*

(Received 28 April 2026, Received in final form 24 July 2026, Accepted 27 July 2026)

Based on the force balance among gravity, surface tension and magnetic force, interfacial instability between ferrofluids and air can be generated under various magnetic fields. The boundary conditions are well discussed to solve the magnetic augmented Navier-Stokes equation in a numerical way. To establish a theoretical model applied for the discontinuous interfacial magnetization jump, the phase field method is applied. The detailed physical meanings of flow field phenomena and interfacial results of magnetic fields are well presented with thorough discussions. Two-dimensional and three-dimensional simulation results of interfacial instability have been systematically studied in this study. The simulation results have a high accordance with the experimental results, which indicates the accuracy of the physical model applied in this study.

Keywords : ferrofluids, interfacial instability, gradient magnetic field

1. Introduction

Ferrofluids, as a kind of special colloidal liquid material, exhibit a unique property that perfectly combines the magnetism of a solid magnet and the fluidity of a liquid. The magnetism in ferrofluids, defined as superparamagnetism with zero coercivity H_c and remanence B_r, is different from that of traditional magnetic materials [1-4]. Based on the fluid magnetic property, ferrofluids are widely applied in many fields, such as magnetic fluid seals [5-9], medical surgery [10], energy absorbers [11] and mineral screening [12-14]. The magnetism of ferrofluids provides them with special properties. One special property is the formation of characteristic spikes in a magnetic field [15-19]. The formation of ferrofluidic spikes in a uniform magnetic field is called Rosensweig instability [20, 21], which was initially discovered and explained by Cowley and Rosensweig [22]. According to Zelazo, the normal magnetic field is the primary driving force for the interfacial instability [23]. In contrast, a tangential magnetic field inhibits the formation of interfacial instability. However, some spikes can still form when the tangential magnetic field is not sufficiently large [23, 24]. Recently, many efforts have been made by other researchers in the simulation of two-dimensional interfacial instability between ferrofluids and other immiscible fluids. The Lattice Boltzmann Method (LBM) is a convenient numerical approach, as it is relatively easy to implement [25]. However, an obvious drawback of LBM is that the physical parameters in the Navier-Stokes equation are transformed into dimensionless quantities that lack direct physical interpretation. LBM effectively solves for the final steady state of the Navier-Stokes equation, but at the cost of losing information about the precise transient dynamics of the fluid. In recent years, Zhang has employed an energy-based method to solve the interfacial instability in ferrohydrodynamics (FHD) [26-30]. Though effective, his method is complicated and difficult to learn and implement. Due to the complexity of that model, some unique parameters in his simulation are difficult to compare with those in our work. Lavrove raised an important point that the static force balance in Rosensweig instability requires an initial surface deformation as initiation [31]. Without initial surface deformation, the liquid surface would remain in its metastable state, remaining flat and smooth. Despite these efforts, the exact mechanism of the magnetization jump, which is attributed to the generation of spikes, remains unclear. Even with the help of initial surface deformation, the simulation convergence is not satisfactory. The mag-

©The Korean Magnetics Society. All rights reserved.
*Corresponding author: Tel: +86 13651206606
E-mail: lidecai@tsinghua.edu.cn

© 2026 Journal of Magnetics

netization jumps at the interface between magnetic ferrofluids and a non-magnetic fluid can still cause significant numerical divergence in the calculation of the magnetic-augmented Navier-Stokes equation. To solve this discontinuity in boundary conditions, the Phase Field Method (PFM) is applied as a major solution [26, 32]. The PFM transforms the sharp discontinuity into a continuous variation across a thin diffuse interface layer. With the help of PFM, the simulation of interfacial instability becomes possible.

In this study, many efforts were made to construct an accurate spike generating process using the finite element method (FEM). The visualized resultant spikes were well distributed in a gradient magnetic field. The force balance between gravity, surface tension, and magnetic forces was scientifically and systematically characterized through numerical methods. The well-distributed three-dimensional spike matrix generated by the gradient magnetic field proved the accuracy and efficiency of our FEM simulation model. In this part of work, the magnetic field was no longer restricted to being uniform. As a result, the periodic spike matrix characteristic of Rosensweig instability was transformed into a "lotus"-like pattern in the gradient field. In addition to the clear distinct spike generation results from interfacial instability, the boundary variation based on the fluid force balance equation was systematically characterized. The bending of magnetic flux lines at the interfacial boundary directly indicates that the boundary exhibits a magnetization jump, which is attributed to spike generation.

2. Results and Discussions

2.1. Governing Equations

The ferrofluids were placed in a container subjected to both a gradient magnetic field and a gravitational field (Fig. 1). Interfacial instability arises at the ferrofluid-air interface. The magnetic flux line distribution depends on the magnetic field intensity $\boldsymbol{H}$ (generated by the permanent magnets) as well as the magnetization of the ferrofluids.

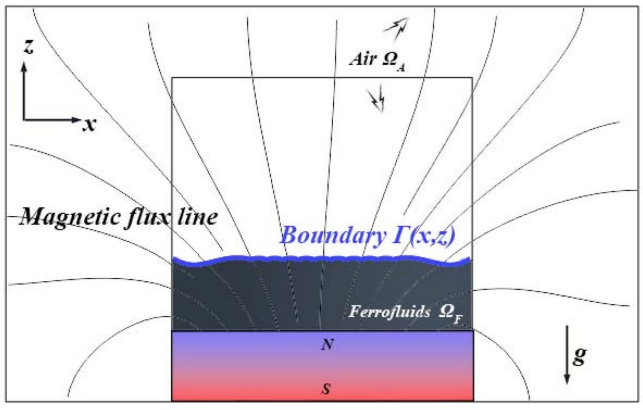


Fig. 1. (Color online) Schematic illustration of magnetic field in simulation zone.

Assuming the total simulation area is defined as an enclosed zone Ω. The ferrofluids area is defined as area Ω_F. The air zone is defined as area Ω_A. The fundamental equations for MHD are Maxwell equations and Navier-Stokes equation. As for Maxwell equations in ferrofluids, there are some principles that always exist in Ω:

$$\nabla \cdot \boldsymbol{B} = 0 \tag{1}$$

$$\nabla \times \boldsymbol{H} = \boldsymbol{J}_S + \frac{\partial \boldsymbol{D}}{\partial t} \tag{2}$$

$$\boldsymbol{B} = \mu_0 (\boldsymbol{H} + \boldsymbol{M}) \tag{3}$$

where parameter $\boldsymbol{B}$ is the magnetic flux density vector, $\boldsymbol{H}$ is the magnetic field intensity vector, $\boldsymbol{J_S}$ is the free current density vector, $\boldsymbol{D}$ is the electric displacement vector, t is the time, μ_0 is the permeability in vacuum, and $\boldsymbol{M}$ is the magnetization vector. Eq. (1) represents flux conservation of magnetic flux density. Eq. (2) is Ampère's circuital law. For ferrofluids in a static magnetic field, the free current density $\boldsymbol{J_S}$, when taken into consideration, is usually equal to the eddy currents generated by the movements of ferrofluids in the magnetic field. The eddy currents are so weak that the influence of $\boldsymbol{J_S}$ in ferrofluids zone Ω_F and air zone Ω_F can be neglected. The electric displacement vector $\boldsymbol{D}$ in the ferrofluids (as well as in air) is always equal to zero because the electric field intensity vector $\boldsymbol{E}$ in ferrofluids is zero in this study ($\boldsymbol{D} = \varepsilon \boldsymbol{E}$, where ε is the permittivity). Therefore, the magnetic field intensity $\boldsymbol{H}$ in the ferrofluids is curl-free ($\nabla \times \boldsymbol{H} = 0$). For $\boldsymbol{H}$ in the ferrofluids, a magnetic scalar potential Φ_m can be conveniently defined:

$$\boldsymbol{H} = -\nabla \Phi_m \qquad \text{in } \Omega_F \text{ and } \Omega_A \tag{4}$$

Based on Eq. (3) and Eq. (4), the magnetic scalar potential Φ_m defined as a kind of potential field should follow the Poisson's equation:

$$\begin{cases} \nabla^2 \Phi_m = \nabla \cdot \boldsymbol{M} \\ \Phi_{m|R=\infty} = 0 \end{cases} \qquad \text{in } \Omega_F \text{ and } \Omega_A \tag{5}$$

where parameter R is the distance from the data point to the origin of the coordinate system. As for Navier-Stokes equation, it becomes strongly nonlinear due to the introduction of magnetic Kelvin force [1, 24]:

$$\rho_{mf}\left(\frac{\partial \boldsymbol{u}}{\partial t}+(\boldsymbol{u}\cdot\nabla)\boldsymbol{u}\right)=-\nabla p+\rho_{mf}\boldsymbol{g}+\eta\nabla^2\boldsymbol{u}+\mu_0\boldsymbol{M}\nabla\boldsymbol{H}$$
$$\text{in } \Omega_F \text{ and } \Omega_A \tag{6}$$

where parameter ρ_{mf} is defined as the density of ferrofluids, t is the time, $\boldsymbol{u}$ is the velocity vector of the velocity field, p is the pressure from the internal source, $\boldsymbol{g}$ is the gravitational acceleration vector, and η is the viscosity of ferrofluids. Eq. (6) is difficult to solve, the efforts done by previous researchers is mainly based on the solving approaches of this complex nonlinear equation. In this study, the FEM is adopted to solve Eq. (6) in a numerical way. The results of time varied flow field and magnetic establish their variation process after placing the ferrofluids into magnetic field.

To calculate the final state of flow field, the boundary conditions should be clarified. To define the boundary Γ between ferrofluids and air, a phase function $f(x, y, z)$ is defined:

$$\phi(x,y,z)=\begin{cases}1 & \text{in air}\\ -1 & \text{in ferrofluids}\end{cases}\quad \text{at } \Gamma \tag{7}$$

Except for the volumetric force balance in Eq. (6), there is another force balance at the interface that determining the final position of interface between ferrofluids and air. This kind of force balance is based on the magnetic augmented Bernoulli equation, which is the same as the Young-Laplace equation at the interfacial boundary Γ [31]:

$$\left(-\mu_0\int_0^H MdH+\frac{\mu_0}{2}(\boldsymbol{e_n}\cdot\boldsymbol{M})^2\right)=\sigma(\nabla\cdot\boldsymbol{e_n})+\rho gZ+P_r \quad \text{at } \Gamma \tag{8}$$

where the parameter $\boldsymbol{e_n}$ is defined as the unit normal vector of interface Γ, σ denotes the surface tension, Z is the vertical coordinate of free surface Γ, P_r is the constant relative pressure. To solve Eq. (8), phase function defined in Eq. (7) is needed. The key problem in solving the Eq. (8) is the solution of unit normal vector $\boldsymbol{e_n}$ of the unknown interface $\Gamma(x, y, z)$. Therefore, we can introduce:

$$\boldsymbol{e_n}=\frac{\nabla\Gamma}{\|\nabla\Gamma\|} \tag{9}$$

Then an implicit equation of $\Gamma(x, y, z)$ can be obtained from Eq. (8) by taking the gradient of both sides of the equation:

$$\mu_0\left(\boldsymbol{M}_x\frac{\partial H_x}{\partial x}+\boldsymbol{M}_y\frac{\partial H_y}{\partial y}+\boldsymbol{M}_z\frac{\partial H_z}{\partial z}\right)$$
$$+\nabla\left(\frac{\mu_0}{2(\nabla\Gamma)^2}\left(\frac{\partial\Gamma}{\partial x}\boldsymbol{M}_x+\frac{\partial\Gamma}{\partial y}\boldsymbol{M}_y+\frac{\partial\Gamma}{\partial z}\boldsymbol{M}_z\right)^2\right)=\sigma\frac{\nabla^2\Gamma}{(\nabla\Gamma)^2}\nabla\Gamma+\rho \tag{10}$$

where parameters $\boldsymbol{M}_x$, $\boldsymbol{M}_y$ and $\boldsymbol{M}_z$ are the magnetization along with x, y and z direction, respectively. Based on Eq. (10), the unknown interface $\Gamma(x, z)$ can be solved by FEM in simulation software Comsol Multiphysics.

2.2. Boundary conditions for coupled field of magnetic field and flow field

In the FEM simulation process, the boundary conditions for the coupled magnetic and flow field system are important for solving the unknown interface $\Gamma(x, y, z)$ in Eq. (10). Since the solution domain encompasses a coupled magnetic-field and flow-field system, the solution process requires integrating the boundary conditions of both fields. The main boundary conditions are presented in Fig. 2. The magnetic boundary conditions are all set as Dirichlet boundary conditions. For the outer boundaries of simulation zone, the magnetic scalar potential Φ_{m2} is all set as 0, which corresponds to the magnetic scalar potential at infinity. As for the bar magnet, the symmetry axis between the two magnetic poles can be set as the zero potential line. The magnetic scalar potential of the north pole at the top of the magnet is defined as Φ_{m1}. The simulation domain for the fluids is artificially established as a rectangular zone presented in Fig. 2. The outer boundary condition of the fluids' zone is set as a wetting wall boundary condition (based on the Young-Laplace equation):

$$\begin{cases}\boldsymbol{u}_n=0\\ \sigma\cos(\theta)=\gamma_{SA}-\gamma_{SF}\end{cases} \tag{11}$$

where parameter $\boldsymbol{u}_n$ is the velocity component normal to the boundary, θ is the contact angle between the two fluids, γ_{SA} is the surface energy density between air and wall, and γ_{SF} is the surface energy density between ferrofluids and wall. In this study, the contact angle θ is

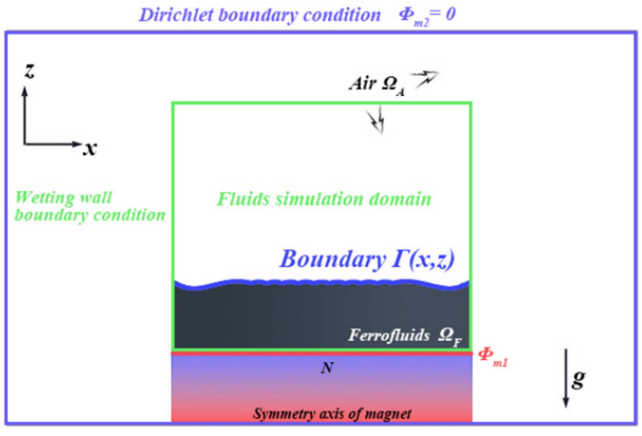


Fig. 2. (Color online) Fundamental boundary conditions settlements in simulation zone.

defined as π/1.8 rad.

2.3. Rosensweig instability: generated from a uniform field intensity H_0.

Once the fluids domains are placed an initially uniform magnetic field intensity $\boldsymbol{H_0}$, the generated interfacial instability between ferrofluids and air is defined as the Rosensweig instability. The Rosensweig instability is also called normal field instability, in which ferrofluids tend to exhibit the periodic repeated spike matrix. Based on the aforementioned physical models, simulation of Rosensweig instability is carried out. The basic setup of the boundary conditions in simulation is presented in Fig. 3. To generate the normal field instability, the magnetic scalar potential Φ_{m1} is settled as a constant, which ensures the constant magnetic field intensity $\boldsymbol{H_1}$ is parallel to the z direction. Besides, the fluids simulation domain is enlarged to match the outer Dirichlet boundary of magnetic simulation region, which ensures the uniformity of the magnetic field. The left and right boundaries are manually set as magnetic insulation boundaries, which indicates that the normal magnetic field intensity at the boundary is set to zero.

At the interface Γ, there is a value jump resulted by the discontinuity of magnetic field intensity $\boldsymbol{H}$ along with the normal direction of interface Γ, as presented in Fig. 3. The discontinuity of $\boldsymbol{H}$ is accorded with the fact that the magnetic field intensity only continues in tangential direction of interface Γ according to the Ampere circuital theorem in Eq. (2). The magnetic force resulting from the magnetization jump, surface tension and gravity constitutes of the major components of forces that establish the Rosensweig instability. The fundamental physical-chemical properties of ferrofluids applied in this study are well provided in Table 1.

Table 1. Fundamental parameters of ferrofluids applied in simulation.

Parameters	Symbol	Value
Density	ρ	1300 kg/m^3
Saturated magnetization	M_s	43.1 kA/m
Interfacial surface tension	σ	30 mN·m
Gravitational acceleration	g	9.8 m/s^2
Viscosity	η	0.1 Pa·s
Initial susceptibility	χ_i	0.75

Once the magnetic field intensity $\boldsymbol{H}$ is applied to the ferrofluids and air, the magnetic surface force originated from the magnetization jump is instantly generated at the interface between ferrofluids and air. Meanwhile, the flow field determination of ferrofluids is timely controlled by the Eq. (6). The non-linear jump value of magnetization $\boldsymbol{M}$ and magnetic field intensity $\boldsymbol{H}$ at the interfacial boundary Γ is participating the establishment of a multi force balance among the gravity, kelvin force and surface tension. With the help of the phase function Φ defined in Eq. (7), the two-phase flow of Rosensweig instability can be well distributed. The interface Γ between ferrofluids and air is manually settled as phase function Φ equals to 0. As presented in Fig. 4, the well distributed spikes' generations are presented. The simulation is based on the 183812 triangular grids with good grid independence. In simulation, the magnetic scalar potential Φ_{m1} and Φ_{m2} are settled as 4000 A and 0 A, respectively. The property of constant critical wave length λ_c has been given by Rosensweig [1, 22, 33]:

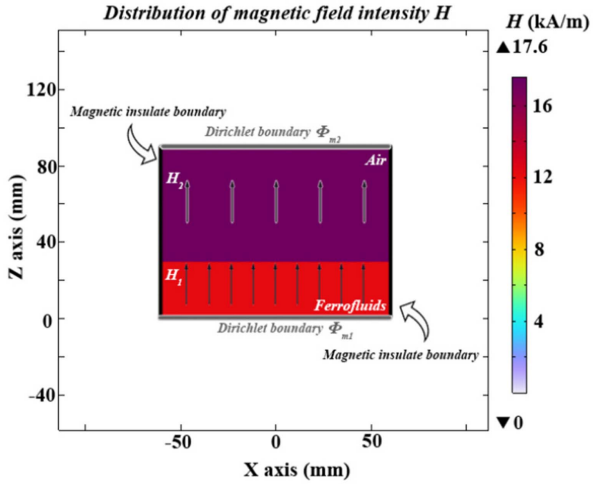


Fig. 3. (Color online) Schematic illustration of magnetic boundary conditions in uniform magnetic field.

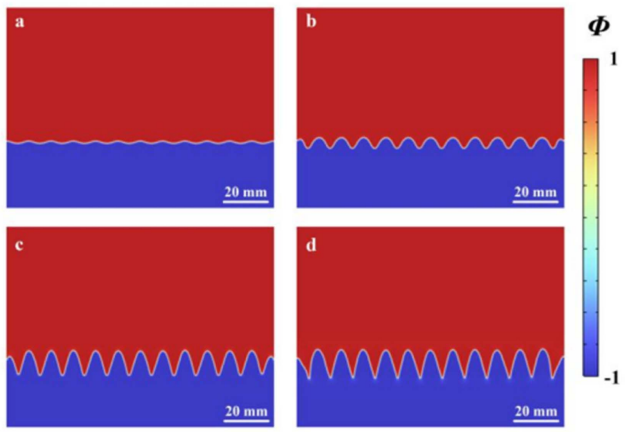


Fig. 4. (Color online) Simulation results of time varied generation of two-dimensional Rosensweig instability. (a) t = 0 s. (b) t = 0.05 s. (c) t = 0.5 s. (d) t = 1.0 s.

$$\lambda_c = 2\pi\sqrt{\frac{\sigma}{\rho g}} \tag{12}$$

where parameter σ is the surface tension, ρ is the density of ferrofluids and g is the gravitational acceleration. As shown in Fig. 4, the critical wave length λ_c in two-dimensional simulation results (λ_c ~ 10 mm) are well fitted to the theoretical results of Rosensweig instability for constant wave length λ_c (λ_c = 9.64 mm).

Except for two-dimensional (2D) Rosensweig instability simulation, three-dimensional (3D) Rosensweig instability has also been characterized in this study. Similar as 2D conditions, the 3D models are established in a rectangular prism, as presented in Fig. 5. The boundary conditions are mainly the same as 2D condition. The four side walls of rectangular simulation region are all settled as magnetic insulate boundaries. The magnetic scalar potential Φ_{m1} and Φ_{m2} are settled as 1550 A and 0 A, respectively. The height h of simulation region (rectangular prism) is settled as 60 mm. The value of as generated magnetic field intensity $\boldsymbol{H}_1$ in 3D results is almost as large as field intensity value in 2D results. In 3D simulation, ferrofluids' zone Occupy bottom one third of the container's volume (simulation rectangular prism). The interface between ferrofluids and air, defined as unknown surface Γ, can be solved by FEM. The definition of surface Γ is the phase function Φ equals to 0. As the critical wave length is deduced as a constant (λ_c = 9.64 mm) in Eq. (12), the peak numbers can be controlled by the edge length L of the simulation flow field (edge length of bottom square of rectangular prism). To construct the stable instability with integar number peaks, the edge length L of simulation zone in Fig. 6 and Fig. 7 are settled as 40 mm and 60 mm, respectively. The value of actual wave length λ_a is slightly larger than the critical wave length λ_c, due to the boundary effects. If the edge length L of 3D simulation region is enlarged to infinity, the actual wave length λ_a would as large as theoretical critical value (λ_c = 9.64 mm).

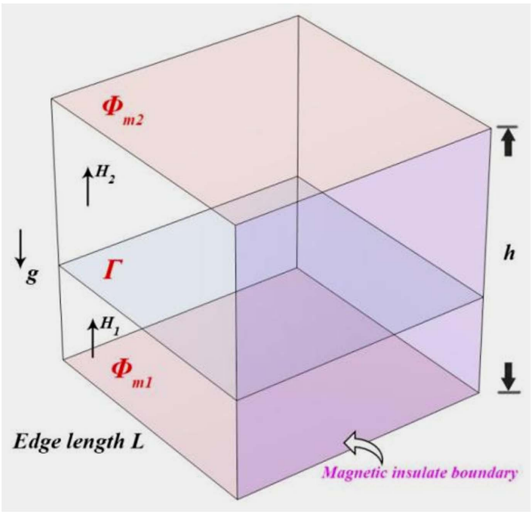


Fig. 5. (Color online) Fundamental definitions of 3D simulation region.

As presented in Fig. 6 and Fig. 7 the interface Γ is gradually evolving into the shape of periodic repeated spikes, which is the unique pattern of spikes of Rosensweig instability. The simulation results in Fig. 6 and Fig. 7 are based on the 1203579 and 4529205 tetrahedral grids with good grid independence, respectively. The matrix of spikes is determined by the boundary conditions and wave lengths of instability spikes. To stimulate the generation of instability, some initial surface deformations are introduced, as presented in Fig. 6a and 7a.

Except for the simulation, some experiments of instability between ferrofluids and air have been designed. The

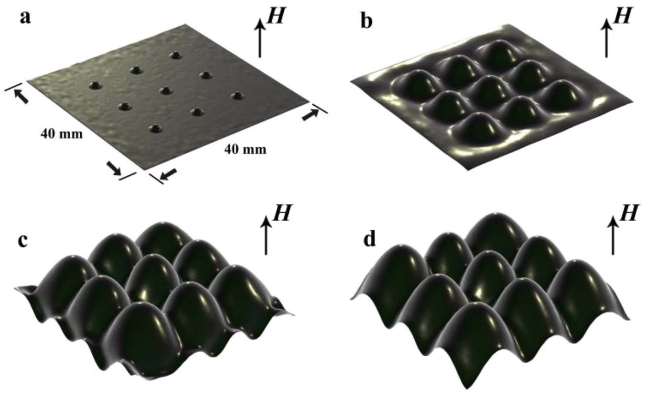


Fig. 6. (Color online) 3D simulation results with edge length L equals to 40 mm of interface Γ at different time. (a) t = 0 s. (b) t = 0.05 s. (c) t = 0.5 s. (d) t = 1.0 s.

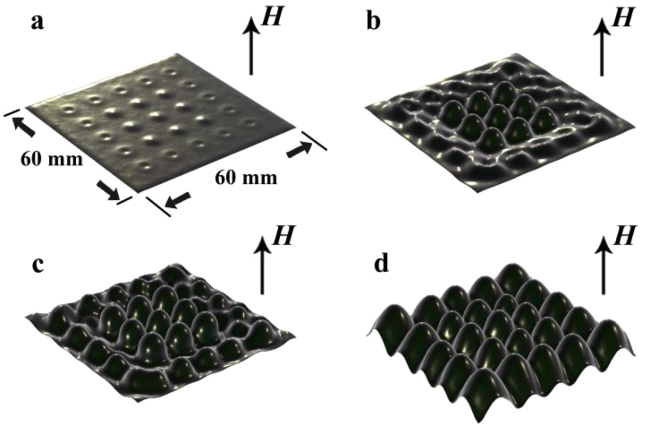


Fig. 7. (Color online) 3D simulation results with edge length L equals to 60 mm of interface Γ at different time. (a) t = 0 s. (b) t = 0.05 s. (c) t = 0.5 s. (d) t = 1.0 s.

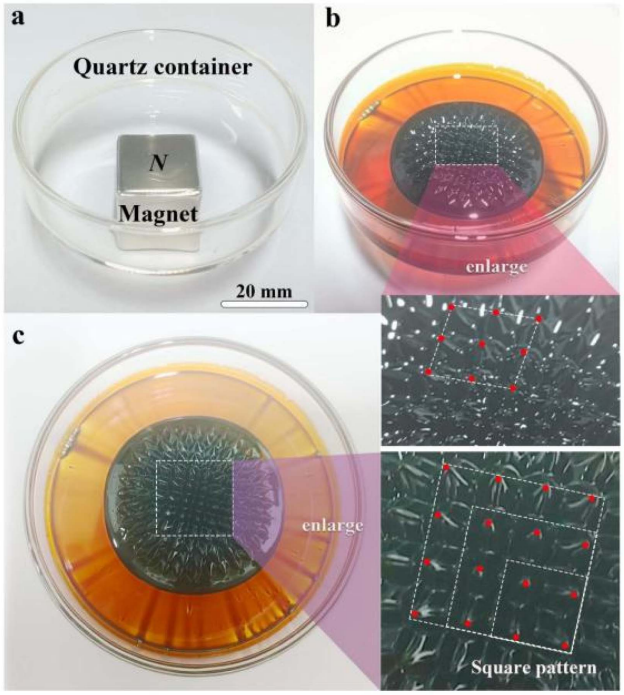


Fig. 8. (Color online) Interfacial instability between ferrofluids and air. (a) experimental environments establishment. (b) side view of instability. (c) top view of instability.

ferrofluids in experiment is kerosene oil based. As presented in Fig. 8a, the quartz container, which is non-magnetic, is placed on a cubic permanent magnet with remanence B_r equals to 300 mT. The value of magnetic field intensity generated by magnet is well accorded to the value of simulation field intensity in Fig. 6 and Fig. 7. Using a cubic magnet with top north pole can generate an approximate uniform magnetic field at the central of container. The as generated magnetic field can make the ferrofluids (saturated magnetization 22.4 kA/m, viscosity 100 mPa·s, density 1300 kg/m^3) to generate the Rosensweig instability within a small central region. As shown in Fig. 8b, the central spikes are exhibiting well periodic pattern of spikes. According to the results in Fig. 8c, the pattern of spikes is showing square pattern, which is well fitted to the simulation results presented in Fig. 6 and Fig. 7.

2.4. The instability in gradient magnetic field

The magnetic field intensity $\boldsymbol{H}$ generated by a certain permanent magnet is always accompany with some gradients of magnetic field intensity $\nabla \boldsymbol{H}$. The vector components tangential to the initial flat ferrofluids surface will have an inhibiting effect in generating the special spikes. If the tangential directional field intensity vector $\boldsymbol{H}_t$ on interface Γ is greatly larger than the normal directional vector of magnetic field intensity $\boldsymbol{H}_n$, the interfacial instability might not occur [23, 24, 34]. Since the tangential directional field intensity $\boldsymbol{H}_t$ can have influence on the shape of spikes in interfacial instability, the simulation of instability has been systematically characterized through the FEM.

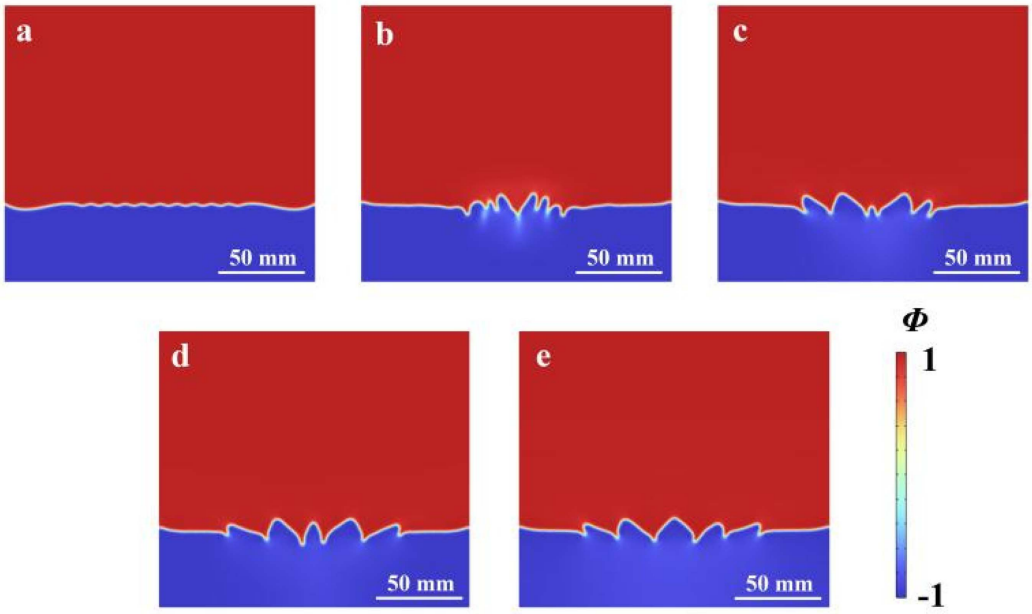


Fig. 9. (Color online) Simulation results of time varied generation of 2D interfacial instability in gradient magnetic fields. The volume ratio between ferrofluids and air is settled as 1/4. (a) t = 0 s. (b) t = 0.05 s. (c) t = 0.5 s. (d) t = 1.0 s. (e) t = 2.0 s.

Based on the aforementioned physical models in chapter 2.1 and 2.2, simulation of gradient magnetic field instability is carried out. Different from the uniform field generated Rosensweig instability (periodic spikes), the magnetic field in part of study is accompanied with a non-zero tangential directional field intensity $\boldsymbol{H}_t$. This kind of magnetic field with radiate flux lines as well as presented in Fig. 1 is defined as "gradient magnetic field". There is a manually defining difference between magnetic scalar potentials in gradient magnetic field and in uniform magnetic field. The magnetic scalar potential Φ_{m1} on the bottom of simulation zone is no longer settled as a constant in Rosensweig instability. The settled magnetic scalar potential Φ_{m1} (A) is defined as:

$$\Phi_{m1} = 12000 \cdot \cos\left(\pi x / (2L)\right)^{0.4} \tag{13}$$

where parameter x (mm) is the coordinate of bottom of simulation flow field zone, L (mm) is the width of simulation flow field zone. The settlement of magnetic scalar potential Φ_{m1} in Eq. (13) is defined based on the potential function of a real magnet. The interface Γ between ferrofluids and air is manually settled as phase function Φ equals to 0. The flow fields shown in Fig. 9 exhibits an establishing process of well-constructed interfacial instability in gradient magnetic field. The simulation is based on 55054 triangular grids and 49706 square grids with good grid independence. The instability shape in this kind of gradient magnetic field is seeming like a blossom lotus, as presented in Fig. 9.

The flow field results are always associated with the magnetic field in simulation of ferrofluids. In Fig. 10, the resultant distribution of magnetic field intensity $\boldsymbol{H}$ related to flow field results in Fig. 9e is presented. In this part of study, the volume ratio between ferrofluids and air is settled as 1/4. As shown in Fig. 10a, the magnetic flux line is all originated from the upper position of magnet, which defined as the magnetic scalar potential Φ_{m1} in Eq. (13). As shown in Fig. 10b, according to the simulation results obtained by model in this study, the magnetic flux line is not that "continuous" at the boundary of the spikes. The boundary flux lines are tending to bending as a "kink" at the solved boundary Γ. The bending flux line at the interface Γ is a symbol of jump values of magnetization which are responsible for the magnetic force at the interface Γ between ferrofluids and air. The enlarged area of a spike provided with a clear boundary of magnetic field intensity between ferrofluids and air zone, indicating that the magnetic field intensity $\boldsymbol{H}$ also has a value jump as well as magnetic flux density $\boldsymbol{B}$ at the interface.

Once the volume ratio between ferrofluids and air decreased to 1/10 accompanied with other basic settings remaining unchanged, as presented in Fig. 11, the generated instability exhibits different shapes of spikes. The interface Γ between ferrofluids and air in simulation is manually settled as phase function Φ equals to 0. As compared with spikes in Fig. 9e, the special spikes in Fig. 11 become sharper and taller. This result can be attributed to the increasing values of magnetic field intensity $\boldsymbol{H}$ and gradients of the magnetic field intensity $\nabla \boldsymbol{H}$ in Fig. 11. The as settled magnetic scalar potential Φ_{m1} is the same as defined in Eq. (13). The ferrofluids in Fig. 11 is under a magnetic field intensity $\boldsymbol{H}$ with larger intensity and gradients, as the ferrofluids are closer to the "pole" of the settled the surface of magnetic scalar potential Φ_{m1}. The as magnetic field intensity $\boldsymbol{H}$ in magnet, which is at the bottom of as defined layer of magnetic scalar potential

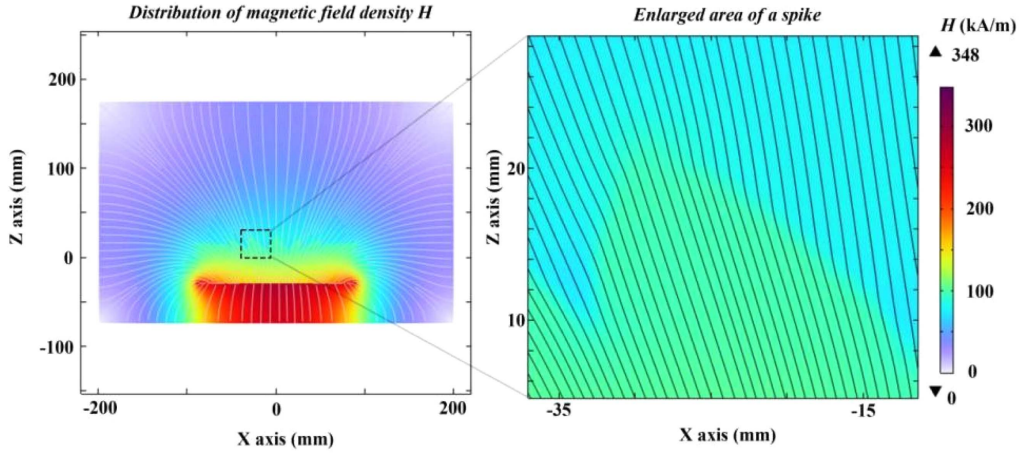


Fig. 10. (Color online) Simulation results magnetic field distribution of 2D interfacial instability in gradient magnetic fields.

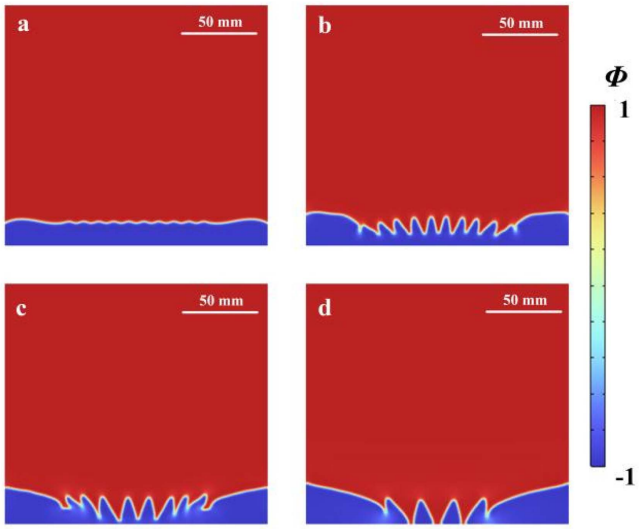


Fig. 11. (Color online) Simulation results of time varied generation of 2D interfacial instability in gradient magnetic fields. The volume ratio between ferrofluids and air is settled as 1/10. (a) t = 0 s. (b) t = 0.05 s. (c) t = 0.5 s. (d) t = 2.0 s.

Φ_{m1}, is as large as 348 kA/m as presented in Fig. 10. The value of magnetic field intensity $\boldsymbol{H}$ is decreased along with the increment of the value of z coordinate, which can be attributed to the divergence of magnetic flux lines.

The interfacial instability simulation results in Fig. 11d are accompanied with complex magnetic field results. In this part of study, the magnetic field characterization is based on the flow field at that moment presented in Fig. 11d. As presented in Fig. 12, the ferrofluids exhibit a well separate spikes' distribution at the center of the simulation area. When characterizing the enlarged area of the central two spikes exhibited in Fig. 12, the magnetic flux lines still bending at the solved interfacial boundary Γ of the spikes. This result of bending flux lines at interfacial boundary Γ is the same as the result in Fig. 10. Except for the magnetic flux bending at the boundary Γ, the spikes are separated as a individual due to insufficiency of ferrofluids. The contact angle between ferrofluids and bottom boundary is settled as π/1.8 rad, which indicates that the wettability between ferrofluids and walls is manually arranged to become poor.

Once the 3D simulation result is considered, some adjustments in magnetic field needed to be taken to generate instability under gradient magnetic field. The original fundamental definitions of simulation zone are defined in Fig. 5. The interface Γ between ferrofluids and air in simulation is manually settled as phase function Φ equals to 0. The magnetic scalar potential Φ_{m1} (A) in this part of study is defined as:

$$\Phi_{m1} = 4200 \cdot \cos\left(\pi \cdot \frac{\sqrt{x^2 + y^2}}{2R}\right)^{0.4} \tag{14}$$

where parameter R = 36 mm is the radius of cylindrical simulation zone. Parameter x and y are the axial coordinate at x and y direction, respectively. The definition domain for x and y are defined as $x \in (-36,36)$ and $y \in (-36,36)$, respectively.

The interface Γ results at certain moments are presented in Fig. 13. The simulation is based on the 7315266 tetrahedral grids with good grid independence. With the help of magnetization jump on the boundary Γ, the time related boundary Γ can be solved by Eq. (6) and Eq. (10). The 3D simulation results are showing ring-cycle distributed spikes. The interfacial instability of spikes is all originated gradient magnetic field, constructing the force balance between magnetic force, gravity and surface tension. It is worthy mention that, the critical wave length of spikes are not that easy to be defined, because the spikes are ring-cycle locating, instead of periodic locating

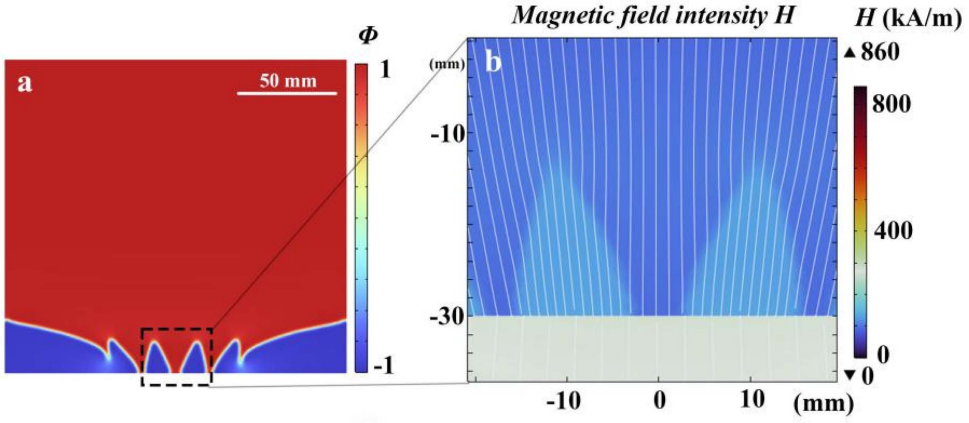


Fig. 12. (Color online) Simulation results magnetic field distribution of 2D interfacial instability at central spikes.

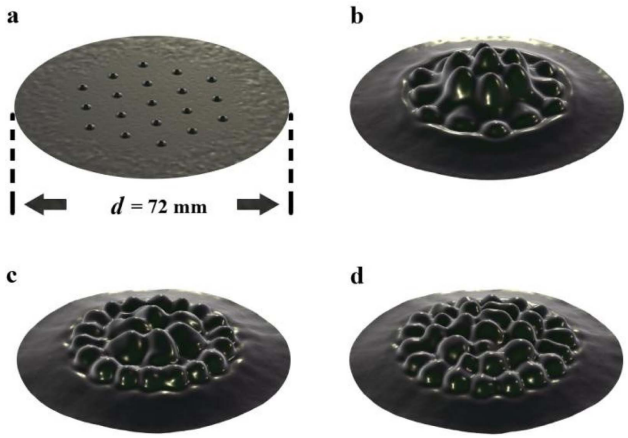


Fig. 13. (Color online) 3D simulation results of the interface Γ in interfacial instability at different time. (a) t = 0 s. (b) t = 0.05 s. (c) t = 0.5 s. (d) t = 1.0 s.



Fig. 14. (Color online) Experimental results of interfacial instability in gradient magnetic field.

on a straight line as in 2D model. Once the cubic magnet in Fig. 8a is replaced by a cylindrical magnet with remanence equals to 230 mT, the ferrofluids can be regarded as located in a gradient magnetic field given in Eq. (14). The experimental results of interfacial instability are well presented in Fig. 14. The experimental results in Fig. 14 shows a ring-cycle distributed spikes, which is highly accorded with the simulation results in Fig. 13d. It indicates that the simulation results of interfacial instability in gradient magnetic field are accurate and useful.

3. Conclusion

In this study, the spike generation resulting from interfacial instability between ferrofluids and air was investigated. The phase field method (PFM) was implemented in COMSOL Multiphysics to examine the generation of interfacial instability. The boundary conditions for both the flow field and magnetic field were well established for various magnetic fields configurations. Boundary conditions are crucial for solving partial differential equations (PDEs), as they not only simplify the solving process but also reduce the degrees of freedom of the PDEs. The Navier-Stokes equation, which currently lacks an analytical solution, relies on boundary conditions to obtain numerical solutions. Interfacial instability between ferrofluids and air was modeled by solving the augmented Navier-Stokes equation with magnetic forces and surface tension. Using this simulation approach, detailed 2D and 3D simulation results of interfacial instability under different magnetic fields are presented.

The main contributions of this study are summarized as follows:

1. Systematic discussion of boundary conditions: The phase field method was employed to address the force continuity deficiency at the interfacial boundary Γ between ferrofluid and air. With appropriate boundary conditions, interfacial instability can be conveniently solved numerically. The bending magnetic flux lines are another manifestation of magnetic pressure originated from magnetization jump.

2. Based on the definition of interfacial boundary Γ in the phase field method (where the phase function Φ equals 0), 3D interfacial instability simulation results between ferrofluids and air are visually presented.

3. The 3D simulation results agree well with experimental data, indicating that both the theoretical model and simulation exhibit high accuracy.

Statement of Originality

The proposed content is original and not involving plagiarism with copyright infringement issues. I hereby declare and guarantee those are true. I would like to declare on behalf of my co-authors that the work described was original research that has not been published previously, and not under consideration for publication elsewhere, in whole or in part.

Data Availability

Data will be available on request.

Acknowledgements

This research is supported by Open Fund Project of National Engineering Research Center of Rubber and Plastic Sealing (2025).

Declaration of Competing Interest

The authors declare that they have no known competing

financial interests or personal relationships that could have appeared to influence the work reported in this paper.

References

[1] R. E. Rosensweig, Ferrohydrodynamics, Courier Corporation, Massachusetts (2013) pp. 177-199.
[2] C. D. Zhang, D. C. Li, W. X. Zhao, S. L. Nie, and J. W. Yang, Applied Materials Today **41**, 102425 (2024).
[3] X. L. Yang, X. M. Geng, M. Shi, Z. Li, and D. C. Li, Vacuum **217**, 112575 (2023).
[4] M. Rasa, European Physical Journal E **2**, 265 (2000).
[5] Y. J. Qiao, D. C. Li, Y. Ge, S. J. Liu, and X. C. Li, Vacuum V**239**, 114366 (2025).
[6] D. Susan-Resiga, V. M. Socoliuc, I. Borbath, T. Borbath, S. C. Tripon, F. Balanean, and L. Vekas, Soft Matter **20**, 6176 (2024).
[7] Y. Liu, X. L. Yang, X. K. Dou, and L. G. Han, Tribol. Int. **193**, 109467 (2024).
[8] Y. Liu, X. L. Yang, X. K. Dou, Y. T. Liu, and Y. Y. Huang, Tribol. Int. **190**, 109054 (2023).
[9] D. C. Li, Y. W. Li, Z. X. Li, and Y. M. Wang, Friction **11**, 1771 (2023).
[10] J. P. Dailey, J. P. Phillips, C. Li, and J. S. Riffle, J. Magn. Magn. Mater. **194**, 140 (1999).
[11] R. Taylor, S. Coulombe, T. Otanicar, P. Phelan, A. Gunawan, W. Lv, G. Rosengarten, R. Prasher, and H. Tyagi, J. Appl. Phys. **113**, 011301 (2013).
[12] L. Li, D. Li, and Y. Guo, J. Magn. Magn. Mater. **629**, 173292 (2025).
[13] A. S. Ivanov and A. F. Pshenichnikov, J. Magn. Magn. Mater. **565**, 170294 (2023).
[14] A. S. Ivanov, A. F. Pshenichnikov, and C. A. Khokhryakova, Phys. Fluids **32**, 112007 (2020).
[15] C. Rigoni, G. Beaune, B. Harnist, F. Sohrabi, and J. V. Timonen, Communications Materials **3**, 26 (2022).
[16] Y. Cao and Z. J. Ding, J. Magn. Magn. Mater. **355**, 93 (2014).
[17] A. N. Spyropoulos, A. G. Papathanasiou, and A. G. Boudouvis, J. Fluid Mech. **870**, 389 (2019).
[18] M. Zahn, J. Nanopart. Res. **3**, 73 (2001).
[19] L. Li, D. C. Li, Z. Q. Qi, L. Wang, and Z. L. Zhang, Chinese Physics B **33**, 034701 (2024).
[20] L. Li, D. C. Li, L. Wang, Z. B. Wang, Z. Q. Liang, and Z. L. Zhang, J. Magn. Magn. Mater. **589**, 171608 (2024).
[21] L. Li, D. C. Li, and Y. Q. Guo, Physica D: Nonlinear Phenomena **489**, 135149 (2026).
[22] M. D. Cowley and R. E. Rosensweig, J. Fluid Mech. **30**, 671 (1967).
[23] R. E. Zelazo and J. R. Melcher, J. Fluid Mech. **39**, 1 (1969).
[24] M. Zahn and R. E. Rosensweig, J. Magn. Magn. Mater. **65**, 293 (1987).
[25] X. Li, Z. Q. Dong, L. P. Wang, X. D. Niu, H. Yamaguchi, D. C. Li, and P. Yu, Appl. Math. Model. **117**, 219 (2023).
[26] G. D. Zhang, S. Zhou, Y. Q. Huang, X. M. He, and X. F. Yang, Journal of Computational Physics. **548**, 114561 (2025).
[27] G. D. Zhang, X. M. He, and X. F. Yang, SIAM J. Sci. Comput. **46**, B77 (2024).
[28] G. D. Zhang, X. M. He, and X. F. Yang, SIAM J. Sci. Comput. **45**, B253 (2023).
[29] G. D. Zhang, X. M. He, and X. F. Yang, J. Comput. Phys. **448**, 110752 (2022).
[30] G. D. Zhang, X. M. He, and X. F. Yang, SIAM J. Sci. Comput. **43**, B167 (2021).
[31] O. Lavrova, G. Matthies, and L. Tobiska, Commun. Nonlinear Sci. Numer. Simul. **13**, 1302 (2008).
[32] J. L. Wang, Z. Y. Xia, L. W. Xu, and Z. Z. Yang, J. Comput. Phys. **547**, 114542 (2026).
[33] J. V. I. Timonen, M. Latikka, L. Leibler, R. H. A. Ras, and O. Ikkala, Science **341**, 253 (2013).
[34] M. I. Shliomis, Soviet Physics Uspekhi **17**, 153 (1974).